*Carcinogenesis*, 2016, Vol. 37, No. 9, 918–928

**doi:10.1093/carcin/bgw071**
Advance Access publication June 22, 2016
Original Manuscript

ORIGINAL MANUSCRIPT

# Dietary flavonoid fisetin increases abundance of high-molecular-mass hyaluronan conferring resistance to prostate oncogenesis

Rahul K.Lall[1,2], Deeba N.Syed[1], Mohammad Imran Khan[1], Vaqar M.Adhami[1], Yuansheng Gong[2], John A.Lucey[2] and Hasan Mukhtar[1,2,*]

[1]Department of Dermatology and [2]Department of Food Science, University of Wisconsin, Madison, WI 53706-1510, USA

*To whom correspondence should be addressed. Tel: +1 608 263 3927; Fax: +1 608 263 5223; E-mail: hmukhtar@dermatology.wisc.edu

## Abstract

We and others have shown previously that fisetin, a plant flavonoid, has therapeutic potential against many cancer types. Here, we examined the probable mechanism of its action in prostate cancer (PCa) using a global metabolomics approach. HPLC–ESI–MS analysis of tumor xenografts from fisetin-treated animals identified several metabolic targets with hyaluronan (HA) as the most affected. Efficacy of fisetin on HA was then evaluated *in vitro* and also *in vivo* in the transgenic TRAMP mouse model of PCa. Size exclusion chromatography-multiangle laser light scattering (SEC-MALS) was performed to analyze the molar mass (Mw) distribution of HA. Fisetin treatment downregulated intracellular and secreted HA levels both *in vitro* and *in vivo*. Fisetin inhibited HA synthesis and degradation enzymes, which led to cessation of HA synthesis and also repressed the degradation of the available high-molecular-mass (HMM)-HA. SEC-MALS analysis of intact HA fragment size revealed that cells and animals have more abundance of HMM-HA and less of low-molecular-mass (LMM)-HA upon fisetin treatment. Elevated HA levels have been shown to be associated with disease progression in certain cancer types. Biological responses triggered by HA mainly depend on the HA polymer length where HMM-HA represses mitogenic signaling and has anti-inflammatory properties whereas LMM-HA promotes proliferation and inflammation. Similarly, Mw analysis of secreted HA fragment size revealed less HMM-HA is secreted that allowed more HMM-HA to be retained within the cells and tissues. Our findings establish that fisetin is an effective, non-toxic, potent HA synthesis inhibitor, which increases abundance of antiangiogenic HMM-HA and could be used for the management of PCa.

## Introduction

Tumor microenvironment plays a major role during prostate cancer (PCa) development. Interactions between the microenvironment and cancer cells are important for migration, metastasis and survival (1). A major component of the extracellular matrix in the tumor microenvironment is glycosaminoglycan, hyaluronan (HA). HA is a non-sulfated, linear polymer composed of repeating disaccharides of glucuronic acid (GlcUA) and *N*-acetyl glucosamine units (GlcNAc) (2). HA is synthesized at the cell surface by the membrane-bound enzyme HA synthase (HAS). Three HAS enzymes HAS1, HAS2 and HAS3 are involved in the production of HA, whereas HA degradation is controlled by hyaluronidases (HYALs), six of which have been identified (3). Increased HA levels in various cancers including PCa correlate with malignant progression and poor survival. These high HA levels are associated with high expression of HAS and low expression of HYALs (4–6).

HA regulates several cellular functions (7,8). The native, high-molecular-mass (HMM)-HA (~$10^7$ Da) can be broken down into smaller fragments in response to glycosidase activity and environmental parameters such as pH and reactive oxygen species (ROS) (9–12). High- and low-molecular-weight forms of HA provoke distinct anti-inflammatory and proinflammatory effects upon binding to CD44 and can deliver either proliferative or antiproliferative signals in various cell types (13,14). Studies

**Received:** January 29, 2016; **Revised:** May 24, 2016; **Accepted:** June 9, 2016

**Abbreviations**

| | |
|---|---|
| 4-MU | 4-methylumbelliferone |
| DMSO | dimethyl sulfoxide |
| DRI | differential refractometer |
| ECM | extracellular matrix |
| ESI | electrospray ionization |
| HA | hyaluronan |
| HAS | HA synthase |
| HMM | high molecular mass |
| HPLC | high-performance liquid chromatography |
| LMM | low molecular mass |
| MALS | multiangle laser light scattering |
| MS | mass spectrometry |
| PBS | phosphate-buffered saline |
| PCa | prostate cancer |
| qPCR | quantitative PCR |
| ROS | reactive oxygen species |
| SEC | size exclusion chromatography |

have shown that HMM-HA exhibited antiangiogenic effects both *in vitro* and *in vivo* (2,15). In contrary, the lower-molecular-mass (LMM)-HA stimulated cell proliferation and exhibited proinflammatory and proangiogenic effects in various studies (14,16,17).

In recent years, considerable progress has been made in identifying a specific inhibitor for HA synthesis and such inhibitor would not only help elucidate the function of HA, but also can be used for treatment of diseases with elevated HA levels (18–22). 4-Methylumbelliferone (4-MU) is one of the well-known and potent HA synthesis inhibitor, and its role has been explored extensively in various cancers (19,21–26), but the $IC_{50}$ of 4-MU to inhibit HA synthesis in prostate and other cancers is as high as 400 μM (~70 μg/ml) (19,22). Therefore, identifying non-toxic inhibitors that effectively suppress HAS levels and its production will be important. Generally considered as non-toxic, dietary flavonoids act as key modulators of signaling pathways and are therefore considered desirable chemopreventive agents (27,28). Fisetin, found in many fruits and vegetables, belongs to the flavonol subgroup of flavonoids and has shown potential against PCa (29–34).

In this study, we identified HA as a unique target of fisetin in PCa cells, tumor xenografts and TRAMP mouse model. We utilized SEC-MALS for a quick, accurate and quantitative determination of different molecular masses of HA both *in vitro* and *in vivo*.

## Materials and methods

### Materials

Fisetin was purchased from Sigma Chemical Co. (St Louis, MO). Antibodies were obtained from Cell Signaling Technology (Danvers, MA), Abcam (Cambridge, MA) and Santa Cruz Biotechnology (Dallas, TX), and a list is provided in Supplementary Table 1, available at *Carcinogenesis* Online. Quantitative PCR (qPCR) primers were synthesized and obtained from DNA synthesis laboratory at the University of Wisconsin Biotechnology Center. The sequences of oligonucleotides used are listed in Supplementary Table 2, available at *Carcinogenesis* Online. Commercially available HA oligos (HA60K-1 and HA200K-1) were purchased from Lifecore Biomedical (Chaska, MN).

### Animals

TRAMP animals were obtained as described previously (35). Housing and care of the animals was approved by the University of Wisconsin's Research Animal Resource Committee in accordance with the NIH Guidelines for the Care and Use of Laboratory Animals.

### Cell culture

Non-tumorogenic RWPE1 (CRL-11609), tumorogenic NB11 (CRL-2851) and NB26 (CRL-2852) cell lines were directly obtained from ATCC (Manassas, VA) in 2013, whereas PC3 (CRL-1435) and DU145 (HTB-81) cell lines were obtained in 2012. ATCC ensures cell lines authenticity using morphology, karyotyping and PCR-based approaches, which include assays to detect cytochrome C oxidase I gene (COI analysis) to rule out interspecies contamination and short tandem repeat DNA profiling to rule out intraspecies contamination as tabulated in Supplementary Table 7, available at *Carcinogenesis* Online. Cell lines were immediately resuscitated upon receipt and frozen in aliquots in liquid nitrogen. Once thawed, early passage cells were cultured within 3 months from a frozen vial of the same batch of cells. Cells were routinely tested to ensure there was no mycoplasma contamination (MycoAlert Mycoplasma Detection Kit, Lonza). RWPE1, NB11 and NB26 cells were cultured in human keratinocyte growth supplement from Thermo-Fisher Scientific (Grand Island, NE), supplemented with HKGS and 1% penicillin–streptomycin. PC3 and DU145 cells were cultured in RPMI 1640 from Gibco (Carlsbad, CA), with 10% fetal bovine serum and 1% penicillin–streptomycin. The cells were then incubated at 37°C with 5% $CO_2$ in a humid environment. For time-dependent studies, cells (70% confluent) were treated with fisetin dissolved in dimethyl sulfoxide (DMSO) (0–40 μM) for specified time points at 37°C in media and harvested for further studies.

### BrdU cell proliferation assay

The BrdU assay from Cell Signaling (Danvers, MA) was used as per the manufacturer's instructions to measure cell proliferation. Absorbance was read at 450 nm using a Synergy 2 multidetection microplate reader (BioTek, VT).

### HPLC–ESI–MS analysis

Aqueous and organic metabolites were isolated from control and fisetin-treated tumor xenograft tissues using a methanol/water and dichloromethane/water extraction as described previously (36). Metabolite extracts (10 μl) were then diluted to 50 μl with 0.1% formic acid in water. Untargeted metabolomics using HPLC–ESI–MS was performed with a 10 μl injection on an Agilent 6210 ESI-TOF mass spectrometer with Agilent 1200 series HPLC (Santa Clara, CA). Solvents were 0.1% formic acid in water (A) and 0.1% formic acid in acetonitrile (B). The HPLC column was an Agilent Zorbax SB C18 1.8 μm, 2.1 mm i.d. × 50 mm length (Santa Clara, CA). Metabolites were gradient-eluted at a flow rate of 0.25 ml/min starting at 2% B with a 1 min hold, ramping to 50% B at 35 min, then to 95% B at 40 min, returning to 2% B at 42 min and re-equilibrating at 2% B for 18 min. Electrospray was performed in positive-ion (+) mode at 3.6 kV and fragmentor at 130V. Metabolite detection was performed over the m/z range 50–1700 by summing 10013 transients/scan (0.89 scans/s). Blank injections (10 μl) of 20% MeOH and 0.08% formic acid in water were made between sample injections.

Raw data acquired using HPLC–ESI–MS system were processed by Xcalibur software that provides an appropriate format for further data analysis. The structured data files were then uploaded on XCMS Online (https://xcmsonline.scripps.edu), a high-quality cloud-based platform linked with METLIN (https://metlin.scripps.edu), to facilitate metabolite identification using a repository of metabolite and tandem mass spectrometry information of known compounds.

### *In vivo* tumor xenograft model

Seven- to eight-week-old athymic (*nu/nu*) male nude mice (Harlan) were xenografted as described previously (30). We selected unique PCa cells NB11 and NB26 for determining the *in vivo* effects of fisetin due to their ability to form rapid and reproducible tumors. After injected, 12 animals were then randomly divided into 2 groups with 6 animals each. The first group of animals received 30 μl i.p. injection of phosphate-buffered saline (PBS)/DMSO (1:1) and served as control. The animals of second group received i.p. injection of fisetin (40 mg/kg ~ 1 mg/animal) in 30 μl of PBS/DMSO (1:1) twice weekly. Tumor sizes were measured twice weekly as described previously (30). All animals were sacrificed when tumors reached a volume of 1200 $mm^3$ in the control group. Samples were collected and stored at –20°C until further analysis.

### Spontaneous PCa progression (TRAMP) model

Eight-week-old transgenic TRAMP mice ($n$ = 27) were randomly divided into two groups for five different time points from 8–12–16–20–24 weeks. Each time point/group contained three animals, respectively. The first group of TRAMP ($n$ = 15) animals received 50 μl PBS/DMSO (1:1) and served

as the control. The second group ($n$ = 12) received fisetin (1 mg/animal) dissolved in 50 µl PBS/DMSO (1:1) thrice weekly, beginning at 8 weeks of age and continued until the animals were 12, 16, 20 and 24 weeks old, respectively. Throughout the experiment, the animals had access to chow diet *ad libitum*.

Animals in all groups were observed weekly for body weight, tumor progression by abdominal palpation and survival. At the termination of the experiment at their respective time points, blood samples were collected by the 'mandibular bleed' and serum was separated and stored at –20°C until further analysis. The prostate was excised under a dissecting microscope and snap frozen in liquid nitrogen for further analysis.

### Western blotting

After treatment with fisetin (40 µM, 48 h), whole cell lysates were prepared and western blot analysis was performed as described previously (29). Densitometric measurements of the bands were done with image analysis software using the Biorad ChemiDoc MP imaging system.

### HA ELISA

Human and Mouse HA ELISA kit were obtained from TSZ ELISA (Waltham, MA) and R&D systems (Minneapolis, MN). These immunoassays have been shown to accurately quantitate HA. Both kits are solid-phase ELISA designed to measure at least 35 kDa HA in biological samples. HA levels in mouse serum and human PCa cells treated with or without fisetin (40 µM, 48 h) were measured according to the manufacturer's protocol.

### RNA isolation and qPCR analysis

Total RNA was extracted from cells and animal tissues using RNeasy kit (Qiagen, Germantown, MD), and reverse transcribed with iScript Reverse transcription supermix kit (Biorad, Hercules, CA). cDNA was amplified in triplicate using gene-specific primers (Supplementary Table 2, available at *Carcinogenesis* Online). Threshold cycle ($C_T$) values obtained from the instrument's software were used to calculate the fold change of the respective mRNAs. $\Delta C_T$ was calculated by subtracting the $C_T$ value of the housekeeping gene from that of the mRNA of interest. $\Delta\Delta C_T$ for each mRNA was then calculated by subtracting the $C_T$ value of the control from the experimental value. Fold change was calculated by the formula $2^{-\Delta\Delta CT}$ (30).

### Intracellular ROS assay

The OxiSelect™ Intracellular ROS Assay Kit obtained from Cell Biolabs Inc. (San Diego, CA) provides a cell-based assay for measuring primarily hydrogen peroxide, along with hydroxyl, peroxyl and other ROS levels within a cell. Cells treated with or without fisetin (40 µM) for specified times were processed as per the manufacturer's instructions. Hydrogen peroxide was used as a positive control in the assay. Fluorescence was evaluated on a Synergy H1 (BioTek) multimode microplate reader at 480/530 nm (excitation/emission) using Gen5 2.0 software (BioTek).

### Immunofluorescence analysis

NB11, NB26, PC3 and DU145 cells treated with fisetin (40 µM, 24 h), xenograft and TRAMP animal slides were incubated with HA antibody as per protocol as described previously (30). After rinsing in PBS tween 20 (PBST), slides were incubated with fluorescent-conjugated secondary antibody at 1:500 dilution in blocking buffer. Slides were then rinsed in PBST, and sections were mounted with ProLong Gold Antifade reagent containing 4′,6-diamidino-2-phenylindole (Invitrogen) and left in dark overnight. Slides were imaged with the Andor Revolution XD spinning-disk confocal microscope using a ×20/×40/1.4 NA oil objective with identical exposures and gains for each antibody stained.

### SEC-MALS analysis

Cells with or without fisetin treatment were collected over time and pooled in order to isolate enough HA to be detected in Size exclusion chromatography-multiangle laser light scattering (SEC-MALS) analysis. HA was isolated using the PEGNAC HA size protocol (available online). This method sequentially removes proteins, nucleic acids and isolate HA from cells, media, tissues or any biological samples. Separation of HA molecular fragments was carried out by SEC-MALS on a Superose 6, 10/300 GL column in series with a Superose 12 and 10/300 GL column (GE Healthcare, Pittsburgh, PA) attached to a Waters HPLC system (Waters Corporation, Milford, MA). A solution containing 20 mM imidazole and 50 mM NaCl at pH 7.0 was used as an eluting buffer. All the samples were filtered through a 0.22 µm filter. Sample injection volume was 100 µl, and nominal flow rate was 0.5 ml/min. The chromatography system consisted of columns, a ultraviolet detector (model 2998; Waters Corporation, Milford, MA) operating at 280 nm, a DAWN-DSP MALS photometer Wyatt Technology, Santa Barbara, CA) fitted with a helium-neon laser (λ = 632.8 nm) and a K-5 flow cell, and a differential refractometer (DRI) detector (model 2414; Waters Corporation, Milford, MA). The electronic outputs of the ultraviolet, DRI and MALS were sent to a Dell computer. The data were processed with ASTRA (version 4.0) software. The DRI response factor was measured by injecting a series of known NaCl concentrations into the detector with the syringe pump. This response factor was obtained from the slope of the linear plot between NaCl concentration and DRI response. The factor to correct the Rayleigh ratio to 90° for instrument geometry was obtained by measuring the LS intensity of filtered (0.025 µm) HPLC quality toluene at 90°. The responses to LS intensity of the photodiodes arrayed around the scattering cell were normalized to the diode at 90° with a bovine serum albumin (BSA) sample (monomeric BSA with a nominal molecular weight of 66 kDa).

### Statistical analysis

Microsoft Excel software was used to calculate the mean and standard error of the mean (SEM). For the HPLC–ESI–MS metabolomics study, a liberal $P$ value of 0.1 was considered significant. Two-tailed, Student's $t$-test was used to assess statistical significance. Data points in all the rest of studies represent mean ± SEM, and $P$ values < 0.05 were considered significant.

## Results

### Identification of HA as a unique target of fisetin in PCa

To identify new biomarkers in PCa, we designed a comprehensive metabolic profiling of fisetin-treated NB11/NB26 tumor xenografts. NB11 and NB26 cells are unique tumorogenic PCa cells derived from non-tumorgenic RWPE1 cells upon exposure to *N*-methyl-*N*-nitrosourea (37). We selected these unique PCa cells, NB11 and NB26, for determining the *in vivo* effects of fisetin due to their ability to form rapid and reproducible tumors. Aqueous and organic extracts were isolated from the tissue samples and analyzed using HPLC–ESI–MS in both positive and negative scan modes. The total ion chromatogram resulted in excellent separation between the two tissue groups ($n$ = 6). The XCMS online analysis of the total ion chromatogram revealed a list of newly identified metabolites. The quasimolecular ions were confirmed and the exact masses of the monoisotopic molecular weights were used to search the METLIN database. Total metabolites identified were 2086, out of which 1203 were downregulated and 883 were upregulated between vehicle control and fisetin-treated NB11 xenografts. Similarly, a total of 2203 metabolites were identified in control versus fisetin-treated NB26 xenografts, out of which 1654 were downregulated and 549 were upregulated (Supplementary Figure 1 and Supplementary Table 8, available at *Carcinogenesis* Online).

To obtain a comprehensive global metabolic signature for this discovery-based approach, we considered a liberal $P$ value of 0.1 as significant for this data set. Among identified metabolites, an m/z of 776.25 stood out as a single metabolite HA (Figure 1A). The relative intensity of the identified HA peak (retention time = 2546.73 min) exhibited a significant decrease in fisetin-treated NB26 xenografts (Figure 1B) and plotted as a function of relative abundance (fold change = 76.09) in both fisetin-treated xenograft groups (Figure 1C). We next performed immunofluorescence staining for HA in NB11 and NB26 tumor

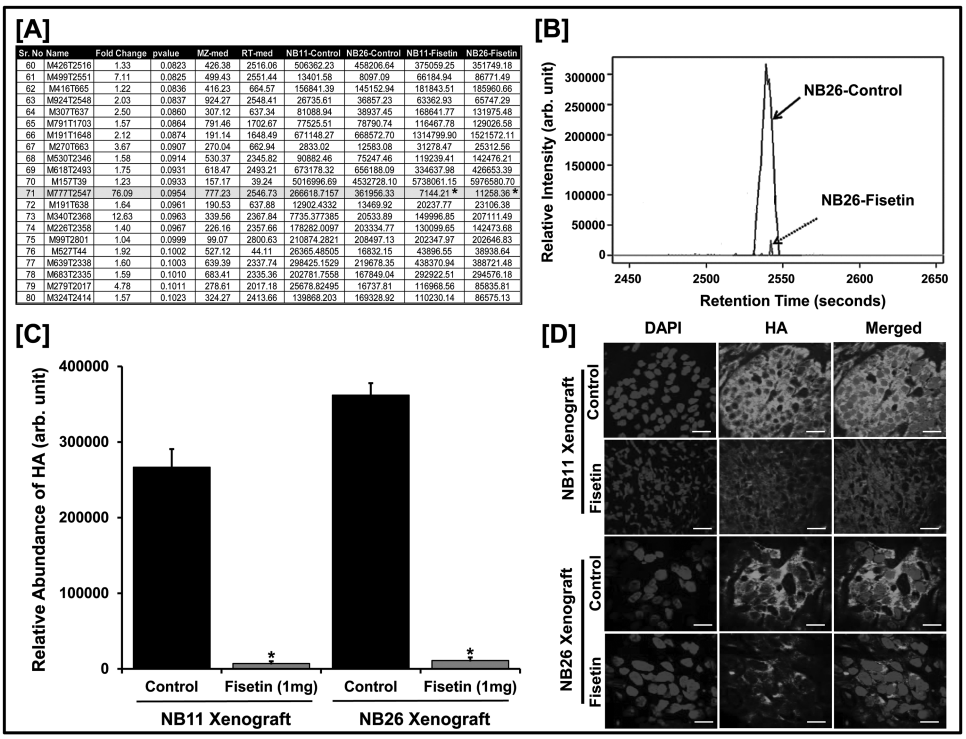


| Sr. No | Name | Fold Change | pvalue | MZ-med | RT-med | NB11-Control | NB26-Control | NB11-Fisetin | NB26-Fisetin |
|---|---|---|---|---|---|---|---|---|---|
| 60 | M426T2516 | 1.33 | 0.0823 | 426.38 | 2516.06 | 506362.23 | 458206.64 | 375059.25 | 351749.18 |
| 61 | M499T2551 | 7.11 | 0.0825 | 499.43 | 2551.44 | 13401.58 | 8097.09 | 66184.94 | 86771.49 |
| 62 | M416T665 | 1.22 | 0.0836 | 416.23 | 664.57 | 156841.39 | 145152.94 | 181843.51 | 185960.66 |
| 63 | M924T2548 | 2.03 | 0.0837 | 924.27 | 2548.41 | 26735.61 | 36857.23 | 63362.93 | 65747.29 |
| 64 | M307T637 | 2.50 | 0.0860 | 307.12 | 637.34 | 81088.94 | 38937.45 | 168641.77 | 131975.48 |
| 65 | M791T1703 | 1.57 | 0.0864 | 791.46 | 1702.67 | 77525.51 | 78790.74 | 116467.78 | 129026.58 |
| 66 | M191T1648 | 2.12 | 0.0874 | 191.14 | 1648.49 | 671148.27 | 668572.70 | 1314799.90 | 1521572.11 |
| 67 | M270T663 | 3.67 | 0.0907 | 270.04 | 662.94 | 2833.02 | 12583.08 | 31278.47 | 25312.56 |
| 68 | M530T2346 | 1.58 | 0.0914 | 530.37 | 2345.82 | 90882.46 | 75247.46 | 119239.41 | 142476.21 |
| 69 | M618T2493 | 1.75 | 0.0931 | 618.47 | 2493.21 | 673178.32 | 656188.09 | 334637.98 | 426653.39 |
| 70 | M157T39 | 1.23 | 0.0933 | 157.17 | 39.24 | 5016996.69 | 4532728.10 | 5738061.15 | 5976580.70 |
| 71 | M777T2547 | 76.09 | 0.0954 | 777.23 | 2546.73 | 266618.7157 | 361956.33 | 7144.21* | 11258.36* |
| 72 | M191T638 | 1.64 | 0.0961 | 190.53 | 637.88 | 12902.4332 | 13469.92 | 20237.77 | 23106.38 |
| 73 | M340T2368 | 12.63 | 0.0963 | 339.56 | 2367.84 | 7735.377385 | 20533.89 | 149996.85 | 207111.49 |
| 74 | M226T2358 | 1.40 | 0.0967 | 226.16 | 2357.66 | 178282.0097 | 203334.77 | 130099.65 | 142473.68 |
| 75 | M99T2801 | 1.04 | 0.0999 | 99.07 | 2800.63 | 210874.2821 | 208497.13 | 202347.97 | 202646.83 |
| 76 | M527T44 | 1.92 | 0.1002 | 527.12 | 44.11 | 26365.48505 | 16832.15 | 43896.55 | 38938.64 |
| 77 | M639T2338 | 1.60 | 0.1003 | 639.39 | 2337.74 | 298425.1529 | 219678.35 | 438370.94 | 388721.48 |
| 78 | M683T2335 | 1.59 | 0.1010 | 683.41 | 2335.36 | 202781.7558 | 167649.04 | 292922.51 | 294576.18 |
| 79 | M279T2017 | 4.78 | 0.1011 | 278.61 | 2017.18 | 25678.82495 | 16737.81 | 116968.56 | 85835.81 |
| 80 | M324T2414 | 1.57 | 0.1023 | 324.27 | 2413.66 | 139868.203 | 169328.92 | 110230.14 | 86575.13 |

**Figure 1.** Identification of HA as a unique target of fisetin. (**A**) Metabolites of NB11 and NB26 xenograft tissues with or without fisetin treatment ($n$ = 6 animals/group) analyzed using untargeted metabolomics (HPLC–ESI–MS) in positive-ion mode. A representative list of 20 metabolites identified from the METLIN database is shown; m/z = 776.25 was identified as HA (Student's t-test; *P ≤ 0.1). For the complete list of metabolites, please see Supplementary Table 8, available at *Carcinogenesis* Online (MS excel file). (**B**) HPLC separation (retention time = 2546.73) and relative intensity of HA metabolite peak identified in NB26 xenografts between control versus fisetin-treated animals. All six biological replicates showed similar analytical separation between the control and treated groups and a representative picture is shown. (**C**) Comparative plot of relative abundance of HA between control and fisetin-treated animal groups in NB11 and NB26 xenografts. Error bars represent mean ± SEM among six biological replicates (fisetin dose was 1 mg/animal thrice weekly; *P ≤ 0.1). (**D**) Representative images showing immunofluorescence for HA between control and fisetin-treated NB11 and NB26 xenografts. Tumor tissues were harvested, and each of the six biological replicates was performed in triplicates for HA staining. Images were captured by a confocal microscope as described in Materials and methods. Scale bar, 30 µm. Magnification for NB11 xenograft images are at ×20 and for NB26 xenograft images at ×40. 4′,6-Diamidino-2-phenylindole (DAPI) was used as a nuclear staining control. Fluorescence intensity was measured and plotted (see Supplementary Figure 2, available at *Carcinogenesis* Online).

tissues and observed that fisetin-treated animals exhibited significantly decreased HA expression as compared with the untreated controls (Figure 1D and Supplementary 2, available at *Carcinogenesis* Online).

## Fisetin decreases intracellular and extracellular HA abundance in PCa cells

We performed immunofluorescence staining for HA in NB11, NB26, PC3 and DU145 PCa cells treated with or without fisetin (40 µM, 48 h). Fluorescence intensity in all four cell types suggested that fisetin-treated cells showed significantly decreased HA expression as compared with the untreated controls (Figure 2A and Supplementary Figure 3, available at *Carcinogenesis* Online). Next, we evaluated intracellular and extracellular HA upon fisetin treatment (40 µM, 48 h) using a solid-phase sandwich human HA ELISA assay. Our data showed that intracellular HA levels significantly decreased in fisetin-treated PCa cells (Figure 2B). Similarly, secreted HA levels in the fisetin-treated group were significantly lower than the untreated control (Figure 2C).

It was further noted that PCa cells secrete more HA in the media and retain less HA within the cell (Figure 2B, Figure 2C). PC3 and NB26 cells treated with or without fisetin (5–40 µM) showed a similar decrease in secreted HA levels in a dose-dependent manner. We found that fisetin decreases HA levels secreted in the media in a dose-dependent manner and enables retention of more HA inside the cell with increasing doses (Supplementary Figure 4A, available at *Carcinogenesis* Online). Also, fisetin treatment (40 µM, 48 h) significantly decreased cell proliferation in NB11 and NB26 cells (Supplementary Figure 4B, available at *Carcinogenesis* Online). Fisetin was able to decrease both intracellular and extracellular HA levels signifying HA as a potential target of fisetin in PCa.

## Fisetin decreases HA levels that are associated with inhibition of disease progression in TRAMP mouse model

The *in vitro* results of NB11/NB26 cells prompted us to look for similar effects of fisetin in another mouse model of PCa. The TRAMP model is a spontaneous PCa progression model that closely mirrors the pathogenesis of human PCa (38,39). Compared with vehicle-treated animals, fisetin-treated animals of 24 weeks exhibited decreased hyperplasia (Supplementary Figure 5A, available at *Carcinogenesis* Online) in the prostate. We found no significant change in body weight of the animals between the vehicle- and fisetin-treated groups as shown (Supplementary Figure 5B, available at *Carcinogenesis* Online), indicating that fisetin is not associated with any significant adverse side effects. We also observed less palpable tumors in fisetin-treated animals when compared with the vehicle-treated controls. Many of the fisetin-treated animals had well-differentiated adenocarcinoma

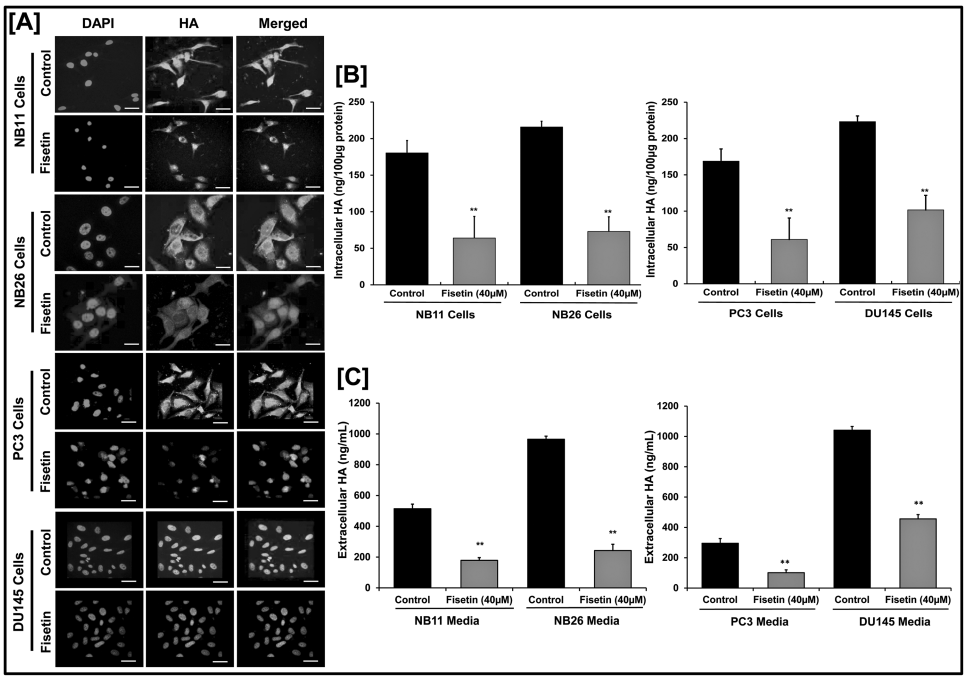


**Figure 2.** Fisetin decreases abundance of HA in PCa cells. (**A**) Representative images showing immunofluorescence for HA in NB11, NB26, PC3 and DU145 cells with or without fisetin (40 µM) treatment for 48 h. Three biological replicates for each were subjected to staining and performed in triplicate. Images were captured by a confocal microscope as described in Materials and methods. Scale bar, 30 µm. Magnification for NB11 images are at ×20 and for NB26 images at ×40. 4′,6-Diamidino-2-phenylindole (DAPI) was used as a nuclear staining control. Fluorescence intensity was measured and plotted (see Supplementary Figure 3, available at *Carcinogenesis* Online). (**B**) Histogram showing intracellular HA levels in NB11, NB26, PC3 and DU145 cells measured with or without fisetin (40 µM) treatment for 48 h. Error bars represent mean ± SEM among three independent experiments/group and each of the three biological replicate was performed in triplicate to measure HA levels using ELISA (**$P \leq 0.01$). All samples were normalized using 100 µg protein of starting whole cell lysates. (**C**) Histogram showing extracellular HA levels secreted in NB11, NB26, PC3 and DU145 cell culture media with or without fisetin treatment (40 µM) for 48 h. Error bars represent mean ± SEM among three independent experiments/group, and each of the three biological replicate was performed in triplicate to measure HA levels using ELISA (**$P \leq 0.01$). All samples were normalized using 1 ml of collected cultured media.

with no evidence of poorly differentiated carcinoma with disease progression (Supplementary Figure 5C, available at *Carcinogenesis* Online).

Next, we performed immunofluorescence staining for HA in TRAMP prostate tissues and compared HA expression intensity among control and fisetin-treated groups. Fluorescence intensity showed that the vehicle-treated control animals demonstrated increased expression with disease progression that was significantly reduced in fisetin-treated animals (Figure 3A, Figure 3B). Next, we evaluated the effect of fisetin on secreted HA levels in TRAMP mouse serum using a mouse HA ELISA. Our results revealed that serum HA levels increased with disease progression and fisetin-treated animals showed significantly lower serum HA levels as compared with the respective controls (Figure 3C).

## Fisetin reduces HA synthesis and degradation enzyme levels *in vitro* and *in vivo*

Previous studies indicate that elevated HAS and HYAL levels are responsible for the high turnover (both synthesis and degradation) of HA in advanced disease state and may cooperate together in cancerous growth. To determine whether fisetin has any effect on HA synthesis and degradation, we evaluated mRNA levels of HAS and HYAL enzymes in NB11 and NB26 cells with or without fisetin treatment (40 µM) for 6 h. Fisetin-treated cells exhibited a significant decrease in HAS and HYAL mRNA levels (Figure 4A). The change in transcriptional levels of HAS and HYALs were reflected in protein expression that were markedly reduced upon fisetin treatment between the two cell types (Figure 4B and Supplementary Figure 4C, available at *Carcinogenesis* Online).

qPCR analysis of PCa tumors of TRAMP tissues revealed a similar significant decrease in HAS2 and HAS3 mRNA levels in fisetin-treated mice as compared with the vehicle-treated controls with increasing weeks of disease progression (Figure 4C). Previous studies have shown that native HA can be broken down into smaller fragments either via enzymatic (via HYALs) or non-enzymatic catabolism (via ROS). Since fisetin decreases enzymatic catabolism via reduction in HYAL levels (Figure 4A, Figure 4B) both *in vitro*/*in vivo*, we investigated the role of non-enzymatic catabolism in fisetin-treated cells by measuring ROS levels in both PC3 and NB26 cells. Increase in ROS levels can breakdown the native HMM-HA into smaller-molecular-weight fragments. Our data show that fisetin increased ROS levels significantly in both PC3 and NB26 cells (Figure 4D).

## Fisetin increases abundance of HMM-HA in PCa cells

In non-diseased conditions, native HA is present as HMM-HA (Mw ~$10^7$ Da), whereas in diseased condition, it gets broken down into LMM-HA. HMM-HA is known to have antiangiogenic properties; however, LMM-HA has shown to be proangiogenic. Since the biological functions of HA is size dependent, we first evaluated the molar mass distribution profile of HA fragments in normal versus cancerous cells. Intracellular HA was collected from normal RWPE1 and PCa PC3 cells by employing the PEGNAC HA size protocol. The isolated HA was then used for SEC-MALS analysis to identify and compare the molar mass of HA fragment in both cell types. The molar mass versus elution

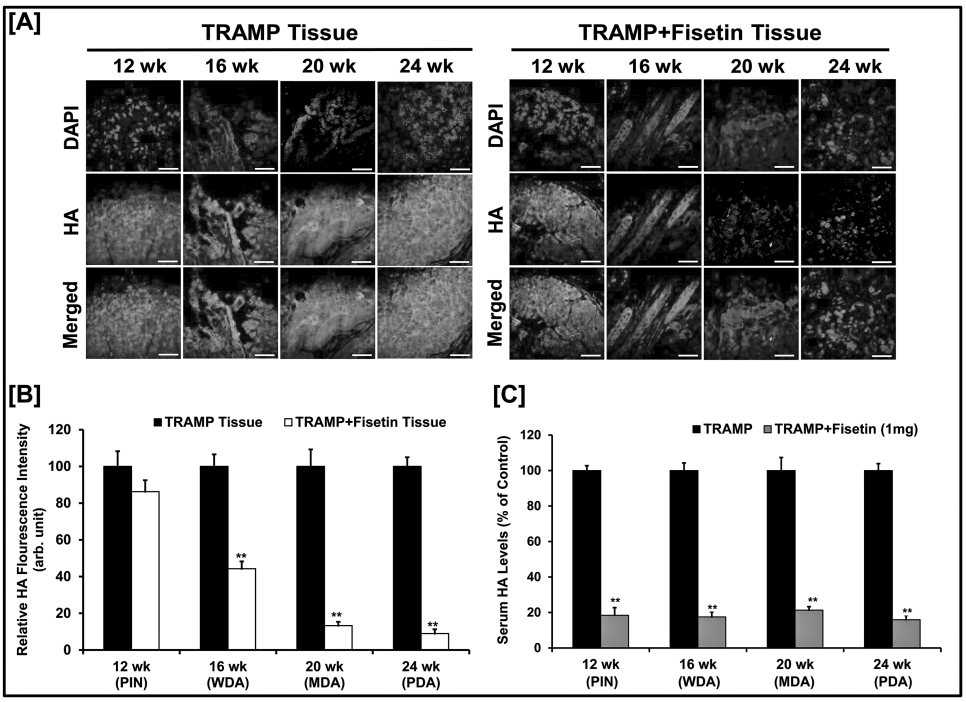


**Figure 3.** Fisetin decreases HA levels *in vivo*. (**A**) Representative images showing immunofluorescence for HA between TRAMP and TRAMP + fisetin groups with increasing age and PCa progression. Prostatic tumor tissues were harvested from three biological replicates and performed in triplicate for HA staining. Images were captured by a confocal microscope as described in Materials and methods. Scale bar, 30 μm; magnification: ×20. 4′,6-Diamidino-2-phenylindole (DAPI) was used as a nuclear staining control. (**B**) HA expression in Figure 3A graphed as relative fluorescence intensity (arbitrary unit) between control and fisetin-treated TRAMP animals with increasing age and PCa progression. Error bars represent mean ± SEM of three biological replicates/group, and each replicate was performed in triplicate for HA staining. Statistical differences were seen in fisetin treatment groups when compared with the respective control group (**P ≤ 0.01). (**C**) Histogram showing HA levels (% control) secreted in TRAMP mice serum between vehicle- and fisetin-treated groups (1 mg/animal; 3 times/week) with increasing stages of PCa progression (PIN, prostatic intraepithelial neoplasia; WDA, well-differentiated carcinoma; MDA, moderately differentiated carcinoma; PDA, poorly differentiated carcinoma). Error bars represent mean ± SEM among three biological replicates/group, and each biological replicate was performed in triplicate for HA levels using ELISA (**P ≤ 0.01).

volume chromatograms of SEC-MALS analysis and the Mw of HA fragments showed that normal RWPE1 cells predominantly exhibited higher levels of HMM-HA fragment cluster and no detectable LMM-HA cluster. In PC3 cells, we observed lower levels of HMM-HA fragment cluster and higher levels of LMM-HA (Figure 5A, Supplementary Table 3, available at *Carcinogenesis* Online) that could contribute to the pro-oncogenic nature of cancer cells.

Next, we determined the effect of fisetin on molecular mass profile of HA fragments in PCa cells. Intracellular and extracellular HA with or without fisetin treatment were isolated from PC3 cells/culture media and analyzed using SEC-MALS. We observed an increased abundance of intracellular HMM-HA fragment cluster in fisetin-treated cells when compared with the untreated control cells. Even the intracellular LMM-HA fragments in fisetin-treated cells were found to have comparatively higher Mw than the untreated control cells (Figure 5B, Supplementary Table 4, available at *Carcinogenesis* Online). Interestingly, we observed that PC3 cells release more HMM-HA in the media, whereas no detectable HMM-HA was secreted in media of fisetin-treated cells suggesting retention of antiangiogenic HMM-HA fragments within the cells.

### Fisetin increases abundance of HMM-HA conferring resistance to prostate oncogenesis in TRAMP mouse model

TRAMP ($n$ = 15) and TRAMP + fisetin ($n$ = 12) animals were selected randomly, and vehicle or fisetin was administered beginning at 8 weeks of age and continued until 24 weeks old, respectively. We measured the HA fragment sizes in vehicle- versus fisetin-treated animals. The light-scattering MALS data in vehicle-treated TRAMP animals showed a decreased abundance of HMM-HA fragment cluster with increased abundance of proangiogenic LMM-HA fragment clusters. Interestingly, in fisetin-treated animals, we observed increased abundance of antiangiogenic HMM-HA fragment clusters and lower abundance of LMM-HA fragment clusters (Figure 6A, Supplementary Table 5, available at *Carcinogenesis* Online). Studies have shown that increased HMM-HA levels are directly associated with resistance to oncogenesis (15,40,41). These results suggest a novel role of fisetin in increasing the abundance of intracellular HMM-HA, which is associated with resistance to PCa progression.

Serum analysis of vehicle-treated TRAMP animals revealed higher secretion of antiangiogenic HMM-HA and lower secretion of LMM-HA fragment clusters. Notably, serum analysis of fisetin-treated animals showed lower secretion of antiangiogenic HMM-HA and higher secretion of proangiogenic LMM-HA fragment clusters (Figure 6B, Supplementary Table 6, available at *Carcinogenesis* Online). Taken together, these findings clearly show that fisetin inhibits the development of PCa in TRAMP mouse model.

## Discussion

Our study demonstrates that fisetin, which is found in many fruits and vegetables, is a potent HA synthesis inhibitor and can be developed for management of PCa. We and others have previously reported that fisetin is an effective proapoptotic

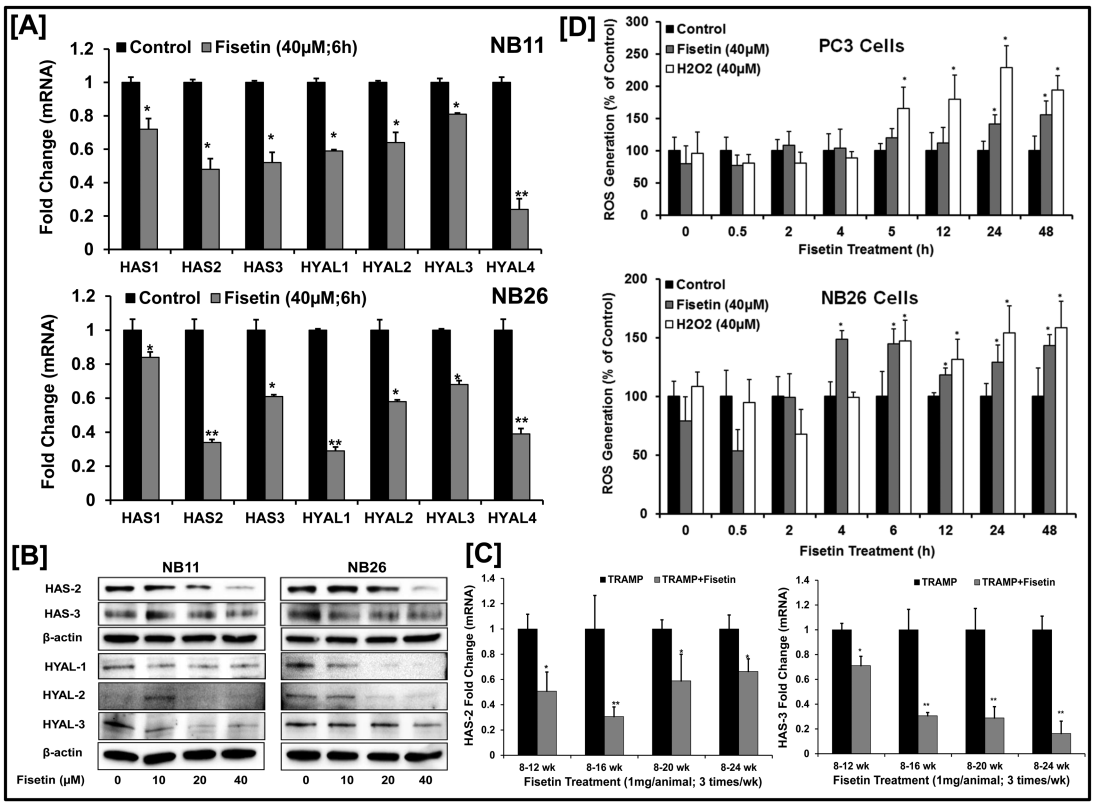


**Figure 4.** Fisetin reduces HA synthesis and degradation enzymes both *in vitro*/*in vivo*. (**A**) Histograms represent relative HAS (1, 2 and 3) and HYAL (1, 2, 3 and 4) mRNA expression in NB11 and NB26 cells treated with or without fisetin (40 μM). Gene expression was measured at 6 h by qPCR and normalized to housekeeping control, GapDH. Error bars represent mean ± SEM among three independent experiments, and each experiment was performed in triplicate. Statistical difference was seen in gene expression on fisetin treatment when compared with the respective control (*$P \leq 0.05$, **$P \leq 0.01$). (**B**) Immunoblot images of NB11 and NB26 cells treated with or without increasing doses of fisetin (0–10–20–40 μM) for 48 h and HAS (2 and 3) and HYAL (1, 2 and 3) protein expression were measured. Three independent experiments were performed, and each experiment was analyzed in triplicate. β-Actin was used as a loading control. Quantitative densitometry was analyzed and plotted (see Supplementary Figure 4, available at *Carcinogenesis* Online). (**C**) Histograms represents relative HAS2 and HAS3 mRNA expression measured by qPCR in prostatic tissues of control and fisetin (1 mg/animal thrice weekly) treated TRAMP animals with increasing age and PCa progression. 18sRNA was used as a housekeeping gene for normalization. Error bars represent mean ± SEM among three independent experiments, and each experiment was performed in triplicates (*$P \leq 0.05$, **$P \leq 0.01$). (**D**) Histogram showing intracellular ROS generation levels (% control) with or without fisetin treatment (40 μM) in a time-dependent manner (0–0.5–2–4–6–12–24–48 h). $H_2O_2$ (40 μM) was used as a positive control. Error bars represent mean ± SEM among three independent experiments, and each experiment was performed in triplicate (*$P \leq 0.05$).

agent with anti-invasive and antiangiogenic properties (29–34). The inhibition of HA synthesis by fisetin is significant considering the fact that targeting the HA pathway with other agents has met with limited success. Only 4-MU has been found to be the most promising till date (19). D-Mannose has shown promise *in vitro* although at very high concentrations of 20 mM (42). Similarly, a curcumin analogue was shown to inhibit HA export from fibroblasts at 5 μM (43); however, antitumor activity of both these agents has not been evaluated at these doses. Sulfated HA has been reported to display antitumor activity by blocking HA signaling, but its oral bioavailability and evidence in experimental *in vivo* models has not yet been evaluated (18). 4-MU, which is a known HA synthesis inhibitor, is effective at high concentrations. The $IC_{50}$ of 4-MU is 400 μM, whereas fisetin inhibits HA synthesis at 40 μM, a 10-fold lower dose. The *in vitro* $IC_{50}$ dose of fisetin translates to 40 mg/kg body weight (~1 mg/day) *in vivo*, which is less than the dose required in humans (1.5–2 g/day) as dietary supplement. At these low doses, fisetin exhibits no detectable toxicity as revealed by xenograft and TRAMP studies. We observed that fisetin (1 mg/animal/day) significantly reduced tumor growth and delayed progression of PCa in the TRAMP mouse model. Fisetin acts as a potent HA synthesis inhibitor and exhibits significant dose advantage when compared with 4-MU both *in vitro* and *in vivo* PCa models.

Accumulation of HA is associated with progression of various cancers including PCa. Nevertheless, there are inconsistent views regarding the significance and relevance of HA secreted in serum. Studies in breast cancer have shown that the total serum HA levels reflect disease progression (44), whereas other studies have shown that the serum HA level does not have any prognostic significance with disease (45). Our results suggest that fisetin significantly decreases both cellular and secreted HA levels in *in vitro*/*in vivo* and shows promise in prevention of other cancers that are associated with increased HA levels.

The concept of HA present inside the cells has met with a lot of skepticism. Several studies have addressed this question, but the actual mechanism of intracellular HA uptake remains elusive. HA is a large molecule synthesized in the plasma membrane; hence, the existence of intracellular HA seems less plausible. However, evidence for intracellular HA has continued to grow over the years, and it is now clear that HA can get into the cells to be catabolized and perhaps perform a number of important cellular functions. HA internalization is tightly regulated and appears to occur simultaneously with increased HA synthesis during cell migration and proliferation (46–52). It seems that

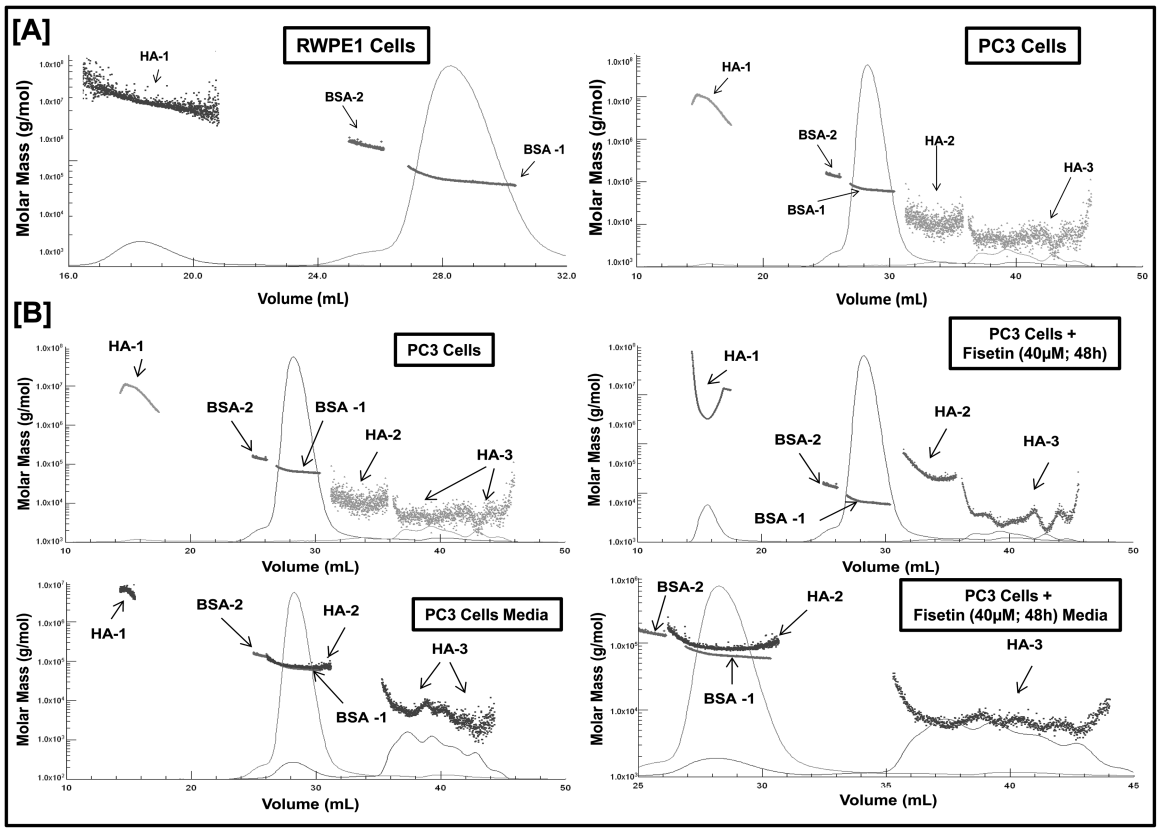


**Figure 5.** Fisetin increases the abundance of HMM-HA in PCa cells. (**A**) SEC-MALS chromatogram showing molar mass distribution profile of HA fragments between normal RWPE1 and cancerous PC3 cells. Refractive index traces (solid line) and the molar mass values calculated from the light scattering data (dotted clusters) are shown, indicating the relative amount and size of HA present in RWPE1 and PC3 cells. The size of HA fragments is represented as HA-1 (HMM-HA clusters), HA-2 (medium-molar-mass HA clusters) and HA-3 (LMM-HA clusters). BSA was used as an internal standard. HA was isolated from three independent experiments and analyzed using SEC-MALS. (**B**) Intracellular and extracellular HA was isolated from cells and culture media with or without fisetin treatment (40 μM; 48 h) and analyzed using SEC-MALS to generate a molar mass distribution profile of HA fragments. Refractive index traces (solid line) and the molar mass values calculated from the light-scattering data (dotted clusters) are shown, indicating the relative amount and size of HA present in PC3 cells (top left) and PC3 cells + fisetin (40 μM, 48 h; top right). Similarly, secreted HA sizes are shown in the cell culture media of PC3 cells (bottom left) and PC3 cells + fisetin (40 μM, 48 h; bottom right). The size of HA fragments is represented as HA-1 (HMM-HA clusters), HA-2 (medium molar mass HA clusters) and HA-3 (LMM-HA clusters). BSA was used as an internal standard. HA was isolated from three independent experiments and analyzed using SEC-MALS.

normal removal of HA from the matrix occurs via CD44 along with HYAL2 activation. HA binds to CD44 and other specific cell surface receptors and gets internalized. Increased HYAL2 results in a cleavage of HMM-HA into smaller fragments, and CD44 is then released and recycled back to the cell surface. Most of the intracellular HA translocated into the cytoplasm or nucleus is primarily low molecular weight (<30 kDa). Our results showed that fisetin treatment significantly decreased hyaluronidase protein levels, especially HYAL1 and HYAL2. Interestingly, we still found HA internalization within the cells even in absence of HYAL2. As observed by others also (50), treatment of cells with the monoclonal antibody to the HA receptor CD44 increased endosomal HA that was significantly decreased upon fisetin treatment (Supplementary Figure 6, available at *Carcinogenesis* Online). We suggest a novel concept that HA internalization in fisetin-treated cells occurs via CD44 alone and is independent of polymer digestion by HYAL2 activation. This significant finding represents the mechanistic aspect of HA internalization upon fisetin treatment.

HAS enzymes synthesize HA, whereas the HYALs degrade it into smaller fragments. This constant HA turnover is important for the maintenance of tissue homeostasis, and ~30% of HA is replaced by newly formed HA every 24 h (53). Importantly, the presence of ROS is known to enhance HA turnover (54–56). Our results show that fisetin treatment significantly inhibits both HAS and HYAL enzymes and halts the synthesis of new HA and also prevents the degradation of previously synthesized HA. Fisetin treatment increased ROS levels *in vitro* but did not enhance HA turnover in PCa cells.

HA is a 'dynamic' molecule with a constant turnover in many tissues via rapid metabolism leading to HA fragments of various sizes: HMM-HA, LMM-HA and o-HA. The innumerable oncogenic functions of HA mainly depend on its molecular size (2,5,9,11,13,14,57). In this study, we used SEC-MALS analysis to accurately measure the molecular distribution of HA size fragments in all biological samples. Although large molecules of HA promote tissue integrity and quiescence, the generation of breakdown products enhances signal transduction, contributing to the pro-oncogenic behavior of cancer cells. Previous studies (15,40,41) have revealed that cancer resistance in naked mole rat derives from the abundant production of HMM-HA. In contrary, LMM-HA has been proven to play a crucial role in breast cancer and seems to be a more promising molecular biomarker than total HA for detecting breast cancer metastasis (57). Our *in vivo*

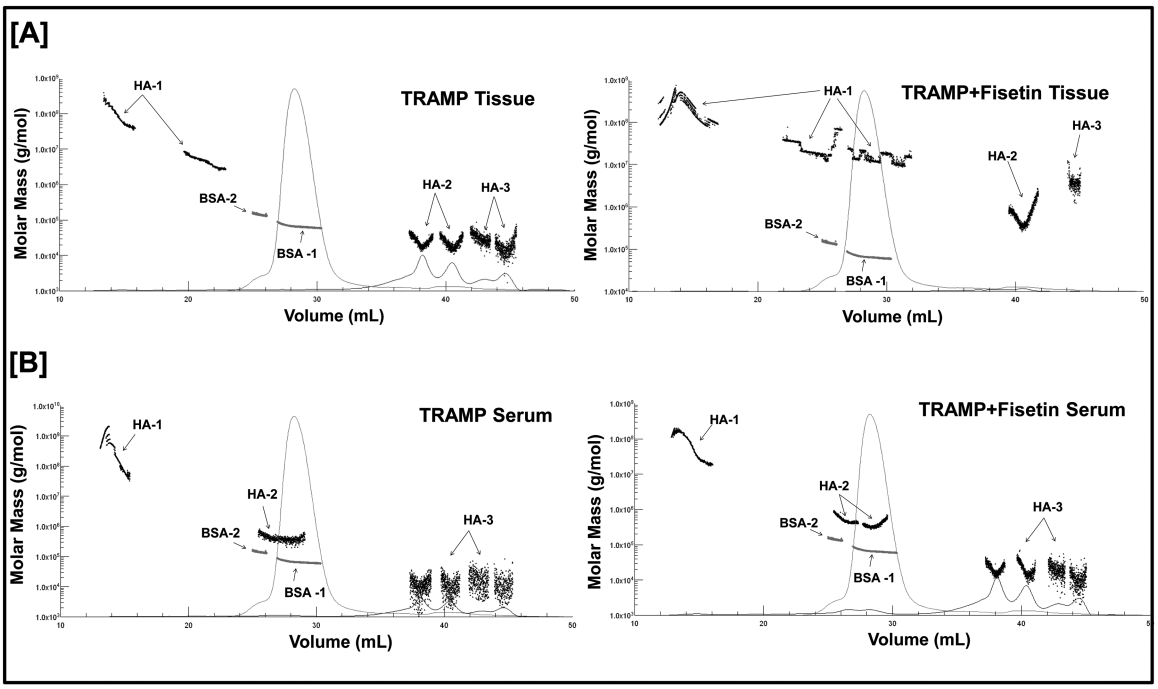


**Figure 6.** Fisetin increases abundance of HMM-HA in TRAMP mouse model. (**A**) Intracellular HA was isolated from tumors (top) of 24 week TRAMP and TRAMP + fisetin animals ($n$ = 3 biological replicates/group) and analyzed using SEC-MALS. Refractive index traces (solid line) and the molar mass values calculated from the light-scattering data (dotted clusters) are shown, indicating the relative amount and size of intact HA present in both animal groups. The size of HA fragments is represented as HA-1 (HMM-HA clusters), HA-2 (medium-molar-mass HA clusters) and HA-3 (LMM-HA clusters). BSA was used as an internal standard. (**B**) Extracellular HA (bottom) was isolated from serum of 24 week TRAMP and TRAMP + fisetin animals ($n$ = 3 biological replicates/group) and analyzed using SEC-MALS. Refractive index traces (solid line) and the molar mass values calculated from the light-scattering data (dotted clusters) are shown, indicating the relative amount and size of secreted HA in serum of both animal groups. The size of HA fragments is represented as HA-1 (HMM-HA clusters), HA-2 (medium-molar-mass HA clusters) and HA-3 (LMM-HA clusters). BSA was used as an internal standard.

results showed that during PCa progression in TRAMP animals, there is increased pool of HMM-HA that further breaks down into LMM-HA. This suggests higher activity of HYAL enzymes leading to higher degradation with disease progression. Increased ROS levels in diseased state may also contribute to the breakdown of HMM-HA into smaller fragments. Upon fisetin treatment, we observed an increase in accumulation of HMM-HA both *in vitro*/*in vivo*. This increase of HMM-HA fragments in presence of fisetin mimics the HA fragment profile of the non-diseased state that unveils a novel effect of fisetin. This effect is because fisetin significantly decreases both HAS and HYAL levels. In this condition, the HA synthesis process is halted and no new HMM-HA is produced. At the same time with reduced activity of HYALs upon fisetin treatment, there seems to be very little or no degradation of the preexisting HMM-HA. Fisetin treatment induces ROS levels, but surprisingly, increased ROS levels do not seem to contribute toward HA degradation as evidenced by larger accumulation of HMM-HA upon fisetin treatment *in vitro*. Hence, the HMM-HA stays intact within the cells and tissues upon fisetin treatment. Another possible reason for this phenomenon could be fisetin's ability to directly or indirectly catalyze and reassemble the LMW-HA fragments into HMW-HA fragments. Interestingly, SEC-MALS analysis of commercially available HA oligos (HA-60K and HA-200K) incubated with fisetin revealed an increase in the molecular weight of the starting HA oligos in a cell-free system (Supplementary Table 9, available at *Carcinogenesis* Online). These preliminary data open up newer promising avenues and suggest fisetin probably possesses the potential to reassemble the smaller HA fragments to larger ones. On the basis of our findings, antiangiogenic HMM-HA is increased in non-diseased states, which undergoes breakdown with progression of disease and larger pool of proangiogenic LMM-HA accumulates. Fisetin reduces the larger pool of LMM-HA and increases the abundance of HMM-HA, which mimics the HA fragment profile of the non-diseased state. The precise mechanism underlying the actual role of fisetin and its ability to directly or indirectly restructure the smaller HA fragments into larger fragments though very promising requires further exploration.

In summary, our study demonstrates fisetin, as a non-toxic, orally bioavailable, potent HA synthesis inhibitor in PCa. Fisetin treatment enables accumulation of a larger pool of antiangiogenic HMM-HA and lowers level of proangiogenic LMM-HA, which leads to reduction of HA signaling. The dose of fisetin used in our *in vivo* studies was comparable with those in human use as a dietary supplement. Hence, by inhibiting HA synthesis, fisetin displays significant potential for prevention and treatment of PCa in preclinical models.

## Supplementary material

Supplementary Tables 1–9 and Figures 1–6 can be found at http://carcin.oxfordjournals.org/

## Funding

United States Public Health Service Grants (RO1 CA160867 to H.M.).

## Acknowledgements

We gratefully acknowledge Cleveland Clinic for using their HA isolation protocol (available online NHLBI # PO1HL107147).

We thank the CORE resource facility at UW-Madison for helping in our confocal imaging studies (National Institutes of Health grant P30 EY016665). We thank Dr G.Barett-Wilt at the UW-Madison Biotechnology Center for his LCMS expertise and assistance.
*Conflict of Interest Statement:* None declared.

## References

1. Sleeman, J.P. et al. (2012) Concepts of metastasis in flux: the stromal progression model. Semin. Cancer Biol., 22, 174–186.
2. Yang, C. et al. (2012) The high and low molecular weight forms of hyaluronan have distinct effects on CD44 clustering. J. Biol. Chem., 287, 43094–43107.
3. Slevin, M. et al. (2007) Hyaluronan-mediated angiogenesis in vascular disease: uncovering RHAMM and CD44 receptor signaling pathways. Matrix Biol., 26, 58–68.
4. Anttila, M.A. et al. (2000) High levels of stromal hyaluronan predict poor disease outcome in epithelial ovarian cancer. Cancer Res., 60, 150–155.
5. Fuchs, K. et al. (2013) Opposing effects of high- and low-molecular weight hyaluronan on CXCL12-induced CXCR4 signaling depend on CD44. Cell Death Dis., 4, e819.
6. Lokeshwar, V.B. et al. (2001) Stromal and epithelial expression of tumor markers hyaluronic acid and HYAL1 hyaluronidase in prostate cancer. J. Biol. Chem., 276, 11922–11932.
7. Simpson, M.A. et al. (2008) Hyaluronan and hyaluronidase in genitourinary tumors. Front. Biosci., 13, 5664–5680.
8. Itano, N. et al. (2002) Abnormal accumulation of hyaluronan matrix diminishes contact inhibition of cell growth and promotes cell migration. Proc. Natl Acad. Sci. USA, 99, 3609–3614.
9. Beasley, K.L. et al. (2009) Hyaluronic acid fillers: a comprehensive review. Facial Plast. Surg., 25, 86–94.
10. Collins, M.N. et al. (2013) Hyaluronic acid based scaffolds for tissue engineering—a review. Carbohydr. Polym., 92, 1262–1279.
11. Rayahin, J.E. et al. (2015) High and low molecular weight hyaluronic acid differentially influence macrophage activation. ACS Biomater. Sci. Eng., 1, 481–493.
12. Stern, R. et al. (2007) The many ways to cleave hyaluronan. Biotechnol. Adv., 25, 537–557.
13. Gao, F. et al. (2010) Hyaluronan oligosaccharides promote excisional wound healing through enhanced angiogenesis. Matrix Biol., 29, 107–116.
14. Gao, F. et al. (2008) Hyaluronan oligosaccharides are potential stimulators to angiogenesis via RHAMM mediated signal pathway in wound healing. Clin. Invest. Med., 31, E106–E116.
15. Tian, X. et al. (2013) High-molecular-mass hyaluronan mediates the cancer resistance of the naked mole rat. Nature, 499, 346–349.
16. Lesley, J. et al. (2000) Hyaluronan binding by cell surface CD44. J. Biol. Chem., 275, 26967–26975.
17. Wang, Y.Z. et al. (2011) CD44 mediates oligosaccharides of hyaluronan-induced proliferation, tube formation and signal transduction in endothelial cells. Exp. Biol. Med. (Maywood), 236, 84–90.
18. Benitez, A. et al. (2011) Targeting hyaluronidase for cancer therapy: antitumor activity of sulfated hyaluronic acid in prostate cancer cells. Cancer Res., 71, 4085–4095.
19. Lokeshwar, V.B. et al. (2010) Antitumor activity of hyaluronic acid synthesis inhibitor 4-methylumbelliferone in prostate cancer cells. Cancer Res., 70, 2613–2623.
20. Nagy, N. et al. (2015) 4-Methylumbelliferone treatment and hyaluronan inhibition as a therapeutic strategy in inflammation, autoimmunity, and cancer. Front. Immunol., 6, 123.
21. Tamura, R. et al. (2014) 4-Methylumbelliferone inhibits ovarian cancer growth by suppressing thymidine phosphorylase expression. J. Ovarian Res., 7, 94.
22. Yates, T.J. et al. (2015) Dietary supplement 4-methylumbelliferone: an effective chemopreventive and therapeutic agent for prostate cancer. J. Natl. Cancer Inst., 107, 85–94.
23. Benitez, A. et al. (2013) Dietary supplement hymecromone and sorafenib: a novel combination for the control of renal cell carcinoma. J. Urol., 190, 285–290.
24. Piccioni, F. et al. (2012) Antitumor effects of hyaluronic acid inhibitor 4-methylumbelliferone in an orthotopic hepatocellular carcinoma model in mice. Glycobiology, 22, 400–410.
25. Uchakina, O.N. et al. (2013) Targeting hyaluronic acid production for the treatment of leukemia: treatment with 4-methylumbelliferone leads to induction of MAPK-mediated apoptosis in K562 leukemia. Leuk. Res., 37, 1294–1301.
26. Wang, R. et al. (2015) Role of hyaluronan and glucose on 4-methylumbelliferone-inhibited cell proliferation in breast carcinoma cells. Anticancer Res., 35, 4799–4805.
27. Lall, R.K. et al. (2015) Dietary polyphenols in prevention and treatment of prostate cancer. Int. J. Mol. Sci., 16, 3350–3376.
28. Sak, K. (2014) Cytotoxicity of dietary flavonoids on different human cancer types. Pharmacogn. Rev., 8, 122–146.
29. Mukhtar, E. et al. (2015) Dietary flavonoid fisetin binds to β-tubulin and disrupts microtubule dynamics in prostate cancer cells. Cancer Lett., 367, 173–183.
30. Khan, M.I. et al. (2014) YB-1 expression promotes epithelial-to-mesenchymal transition in prostate cancer that is inhibited by a small molecule fisetin. Oncotarget, 5, 2462–2474.
31. Adhami, V.M. et al. (2012) Dietary flavonoid fisetin: a novel dual inhibitor of PI3K/Akt and mTOR for prostate cancer management. Biochem. Pharmacol., 84, 1277–1281.
32. Suh, Y. et al. (2010) Fisetin induces autophagic cell death through suppression of mTOR signaling pathway in prostate cancer cells. Carcinogenesis, 31, 1424–1433.
33. Khan, N. et al. (2008) A novel dietary flavonoid fisetin inhibits androgen receptor signaling and tumor growth in athymic nude mice. Cancer Res., 68, 8555–8563.
34. Khan, N. et al. (2008) Fisetin, a novel dietary flavonoid, causes apoptosis and cell cycle arrest in human prostate cancer LNCaP cells. Carcinogenesis, 29, 1049–1056.
35. Adhami, V.M. et al. (2012) Oral infusion of pomegranate fruit extract inhibits prostate carcinogenesis in the TRAMP model. Carcinogenesis, 33, 644–651.
36. Want, E.J. et al. (2013) Global metabolic profiling of animal and human tissues via UPLC-MS. Nat. Protoc., 8, 17–32.
37. Webber, M.M. et al. (2001) Human cell lines as an *in vitro/in vivo* model for prostate carcinogenesis and progression. Prostate, 47, 1–13.
38. Gingrich, J.R. et al. (1997) Androgen-independent prostate cancer progression in the TRAMP model. Cancer Res., 57, 4687–4691.
39. Gingrich, J.R. et al. (1996) Metastatic prostate cancer in a transgenic mouse. Cancer Res., 56, 4096–4102.
40. Fisher, G.J. (2015) Cancer resistance, high molecular weight hyaluronic acid, and longevity. J. Cell Commun. Signal., 9, 91–92.
41. Seluanov, A. et al. (2009) Hypersensitivity to contact inhibition provides a clue to cancer resistance of naked mole-rat. Proc. Natl Acad. Sci. USA, 106, 19352–19357.
42. Jokela, T.A. et al. (2013) Mannose reduces hyaluronan and leukocytes in wound granulation tissue and inhibits migration and hyaluronan-dependent monocyte binding. Wound Repair Regen., 21, 247–255.
43. Prehm, P. (2013) Curcumin analogue identified as hyaluronan export inhibitor by virtual docking to the ABC transporter MRP5. Food Chem. Toxicol., 62, 76–81.
44. Delpech, B. et al. (1990) Serum hyaluronan (hyaluronic acid) in breast cancer patients. Int. J. Cancer, 46, 388–390.
45. Ponting, J. et al. (1992) Prognostic relevance of serum hyaluronan levels in patients with breast cancer. Int. J. Cancer, 52, 873–876.
46. Brecht, M. et al. (1986) Increased hyaluronate synthesis is required for fibroblast detachment and mitosis. Biochem. J., 239, 445–450.
47. Evanko, S.P. et al. (1999) Intracellular localization of hyaluronan in proliferating cells. J. Histochem. Cytochem., 47, 1331–1342.
48. Hascall, V.C. et al. (2004) Intracellular hyaluronan: a new frontier for inflammation? Biochim. Biophys. Acta, 1673, 3–12.
49. Ripellino, J.A. et al. (1988) Light and electron microscopic studies on the localization of hyaluronic acid in developing rat cerebellum. J. Cell Biol., 106, 845–855.
50. Tammi, R. et al. (2001) Hyaluronan enters keratinocytes by a novel endocytic route for catabolism. J. Biol. Chem., 276, 35111–35122.
51. Tammi, R. et al. (1991) Correlations between hyaluronan and epidermal proliferation as studied by [3H]glucosamine and [3H]thymidine incor-

porations and staining of hyaluronan on mitotic keratinocytes. Exp. Cell Res., 195, 524–527.
52. Vigetti, D. et al. (2009) Modulation of hyaluronan synthase activity in cellular membrane fractions. J. Biol. Chem., 284, 30684–30694.
53. Fox, S.B. et al. (1994) Normal human tissues, in addition to some tumors, express multiple different CD44 isoforms. Cancer Res., 54, 4539–4546.
54. Hrabárová, E. et al. (2012) Free-radical degradation of high-molar-mass hyaluronan induced by ascorbate plus cupric ions: evaluation of anti-oxidative effect of cysteine-derived compounds. Chem. Biodivers., 9, 309–317.
55. Hrabarova, E. et al. (2011) Pro-oxidative effect of peroxynitrite regarding biological systems: a special focus on high-molar-mass hyaluronan degradation. Gen. Physiol. Biophys., 30, 223–238.
56. Soltés, L. et al. (2006) Degradative action of reactive oxygen species on hyaluronan. Biomacromolecules, 7, 659–668.
57. Wu, M. et al. (2015) A novel role of low molecular weight hyaluronan in breast cancer metastasis. FASEB J., 29, 1290–1298.